Available online at www.sciencedirect.com

ScienceDirect

Energy Procedia 161 (2019) 480–488

Energy Procedia

www.elsevier.com/locate/procedia

2nd International Conference on Sustainable Energy and Resource Use in Food Chains, ICSEF 2018, 17-19 October 2019, Paphos, Cyprus

Numerical study of the thermohydraulic performance of printed circuit heat exchangers for supercritical CO_2 Brayton cycle applications

Lei Chai* and Savvas A Tassou

Brunel University London, Institute of Energy Futures, RCUK Centre for Sustainable Energy use in Food chains (CSEF), Uxbridge, UB8 3PH, United Kingdom

Abstract

The printed circuit heat exchanger is currently the preferred type of recuperative heat exchanger for the supercritical CO_2 Brayton cycle due to its highly compact construction, high heat transfer coefficients and its ability to withstand high pressures and temperatures. This paper employs a three-dimensional numerical model to investigate the thermohydraulic performance of supercritical CO_2 flow in a printed circuit heat exchanger. This numerical model considers entrance effects, conjugate heat transfer, real gas thermophysical properties and buoyancy effects. The inlet temperature and pressure are 100 °C/150 bar on the cold side and 400 °C/75 bar on the hot side while the mass flux is varied from 254.6 to 1273.2 kg/(m^2·s). The overall performance of the heat exchanger and comparisons of local heat transfer and friction pressure drop with predictions from the empirical correlations are presented and discussed. Overall, this paper provides useful information that can be employed in the design of recuperators for supercritical CO_2 Brayton cycle applications.

Keywords: Numerical simulation; printed circuit heat exchanger; thermohydraulic performance; supercritical CO_2 Brayton cycle.

* Corresponding author. Tel.: +44-189-526-5834.
E-mail address: Lei.Chai@brunel.ac.uk

10.1016/j.egypro.2019.02.066

Nomenclature

A	area, m^2	x, y, z	three coordinates shown in Fig. 1, m
D	hydraulic diameter, m	Greek letters	
f	friction factor	ΔT	temperature difference, K
G	mass flux, kg/(m^2·s)	ρ	density, kg/m^3
h	heat transfer coefficient, W/(m^2·K)	λ	thermal conductivity, W/(m·K)
L	length, m	μ	dynamic viscosity, Pa·s
Nu	Nusselt number	*Subscripts*	
p	pressure, Pa	i	inlet
q	heat flux, W/m^2	f	fluid, fiction
Q	heat transfer rate, W	o	outlet
Re	Reynolds number	z	local
T	temperature, K	w	wall
U	overall heat transfer coefficient, W/(m^2·K)		

1. Introduction

Globally, the increase of electrical energy demands and environmental concerns make the supercritical CO_2 Brayton cycle an alternative to steam and air cycles, due to its advantage of small size, use of standard materials, and improved electrical-power-conversion efficiency. Such cycle design usually applies a recuperator between the expander exhaust and the compressor exhaust to improve the cycle efficiency by reducing the amount of heat lost in the CO_2 cooler and increasing the amount of working fluid in the CO_2 heater [1]. Among the various types of recuperator, printed circuit heat exchanger (PCHE) is preferable due to its highly compact construction, exceptionally high heat transfer coefficients, high pressure capability and wide range of operating temperatures.

PCHE is a promising technology of compact heat exchanger, and was originally invented at the University of Sydney in the early 1980s. Two advanced technologies are applied to manufacture the PCHE: photo etching and diffusion bonding. Flat metal plates are photo-chemically etched with specific design patterns and joined by a diffusion-bonding process to form a compact, strong, all-metal structure containing complex internal passages that allow for precise flow control, fluid manifolding and metering features [2]. For supercritical CO_2 Brayton cycle, the PCHE need to accommodate a higher temperature and significant pressure differentials between the exchanging fluids, and its heat transfer and pressure drop (thermohydraulic) characteristics are key performance of a recuperator. Kruizenga et al. [3, 4] and Li et al. [5] measured the heat transfer and pressure drop data of a PCHE with straight channels. They focused on the supercritical CO_2 in the temperature range from 10 to 100 °C under cooling conditions.

For a detailed investigation into the thermohydraulic performance of supercritical CO_2 in PCHE, this paper presents a three-dimensional numerical model considering entrance effects, conjugate heat transfer, real gas thermophysical properties and buoyancy effects. The local and average thermohydraulic performance of supercritical CO_2 in both hot and cold sides of the PCHE are presented.

2. Computational method

A three-dimensional physical model containing two straight microchannels and surrounding solid is established in the present work as shown in Fig. 1. The cross section of the channels is semicircular with a diameter of 2 mm, and the channel length is 272 mm. The channel pitch is 2.54 mm in the x direction and 3.26 mm in the y direction. The cold supercritical CO_2 flows in the upper channel and the hot flows in the lower channel. Due to the significant variations of thermophysical properties of supercritical CO_2 in the test pressure and temperature conditions, the NIST real gas thermophysical properties are used in this present work and the buoyant effect is enclosed. The standard k-ε model is adopted for the turbulent simulation.

$$\frac{\partial}{\partial x_i}(\rho k u_i) = \frac{\partial}{\partial x_j}\left[\left(\mu + \frac{\mu_t}{\sigma_k}\right)\frac{\partial k}{\partial x_j}\right] + G_k + G_b - \rho\varepsilon \tag{1}$$

$$\frac{\partial}{\partial x_i}(\rho \varepsilon u_i) = \frac{\partial}{\partial x_j}\left[\left(\mu + \frac{\mu_t}{\sigma_k}\right)\frac{\partial \varepsilon}{\partial x_j}\right] + G_{1\varepsilon}\frac{\varepsilon}{k}(G_k + G_{3\varepsilon}G_b) - G_{2\varepsilon}\rho\frac{\varepsilon^2}{k} \tag{2}$$

where G_k and G_b represent the generation of turbulence kinetic energy due to the mean velocity gradients and buoyancy, α_k and α_ε are the inverse effective Prandtl numbers for k and ε, respectively.

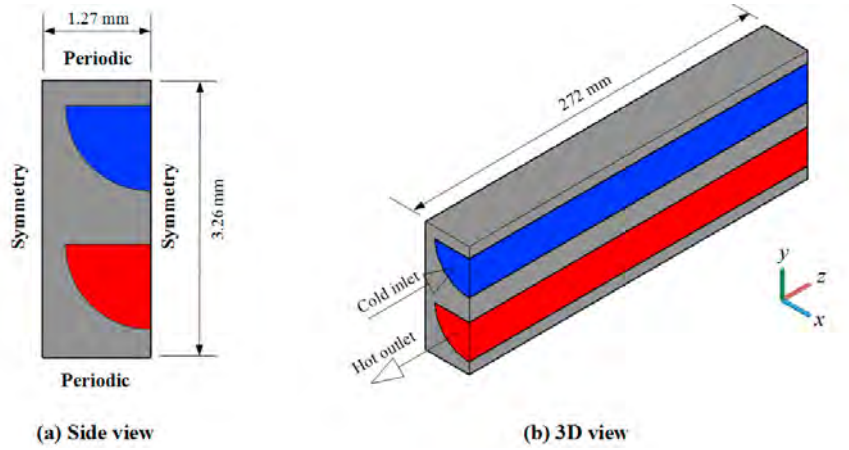

Fig. 1. Geometry and boundary condition of PCHE analysis model: (a) Side view. (b) 3D view.

The numerical calculation is carried out by software ANSYS Fluent 17.0. The thermophysical properties of supercritical CO_2 come from REFPROP v9.1, which is activated and dynamically loaded into the solver. Mass-flow-inlet boundary with constant temperature is employed in the inlets of the two channels. The mass flux balances for the two inlets, varying from 254.6 to 1273.2 kg/(m^2·s). The inlet temperature is 100 °C for the cold side and 400 °C for the hot side. Pressure-outlet boundary is employed in the outlets of the two channels, 150 bar for the cold side and 75 bar for the hot side. Thermally-periodic boundary at the top and bottom surfaces and symmetry boundary at the left and right surfaces allow the simulation results to be easily extended to the entire heat exchanger. The SIMPLEC algorithm is applied to solve the governing differential equations for the velocity, pressure and temperature fields in the control volume. The convergence criteria are the normalised residuals of all variables in momentum and energy equations less than 10^{-5}. A grid independence test is checked using several different mesh sizes and a total number of generated meshes about 1.844 million is used for this present work.

3. Data acquisition

The parameters relevant to the local and average thermohydraulic performances are listed in Table 1, where G is the mass flux, D is the hydraulic diameter, q_z, $T_{w,z}$ and $T_{f,z}$ are the local heat flux, local wall temperature and local fluid temperature respectively at a fixed z plane; ρ_z, μ_z and $\lambda_{f,z}$ are the local density, dynamic viscosity and thermal conductivity respectively of the fluid; dp_f/dz represents the pressure gradient due to friction, and L is the channel length.

The overall heat transfer coefficient is calculated by

$$U = \frac{Q}{A\Delta T_m} \tag{3}$$

$$\Delta T_m = \frac{(T_{hi} - T_{co}) - (T_{ho} - T_{ci})}{\ln(\frac{T_{hi} - T_{co}}{T_{ho} - T_{ci}})} \quad (4)$$

where Q, is the heat transfer rate, ΔT_m is the log mean temperature difference, T_{hi}, T_{ho}, T_{ci} and T_{co} are the temperatures of inlet and outlet of hot and cold sides respectively.

Table 1. Parameters relevant to the local and average thermohydraulic performance.

Local thermohydraulic parameters		Average thermohydraulic parameters	
$Re_z = \frac{GD}{\mu_z}$	(3)	$\overline{Re} = \frac{\int_0^L Re_z dz}{L}$	(7)
$h_z = \frac{q_z}{T_{w,z} - T_{f,z}}$	(4)	$\overline{h} = \frac{\int_0^L h_z dz}{L}$	(8)
$Nu_z = \frac{h_z D}{\lambda_{f,z}}$	(5)	$\overline{Nu} = \frac{\int_0^L Nu_z dz}{L}$	(9)
$f_z = \frac{2\rho_z D}{G^2} \frac{dp_f}{dz}$	(6)	$\overline{f} = \frac{\int_0^L f_z dz}{L}$	(10)

4. Results and discussion

4.1. Local thermohydraulic performance

Fig. 2 presents the temperature and velocity contours at z = 136 mm and G = 763.9 kg/(m^2·s). Large temperature and velocity gradients are found for supercritical CO_2. The average temperature of supercritical CO_2 in this cross section is 159.4 °C (432.55K) on the cold side and 302.4 °C (575.55K) on the hot side. The corresponding temperature difference between the fluid and wall is 69.2 K on the cold side and 64.8 K on the hot side. The average velocity of the supercritical CO_2 in this cross section is 3.4 m/s on the cold side and 10.8 m/s on the hot side.

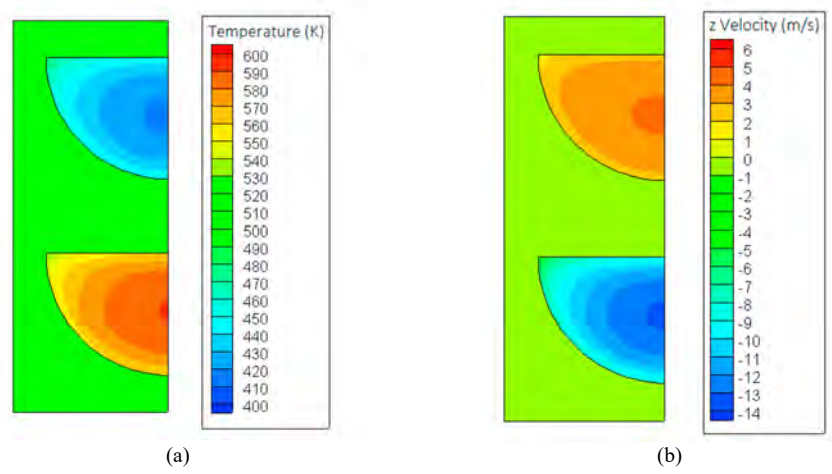

Fig. 2. Computational plots (z = 136 mm, G = 763.9 kg/(m^2·s)): (a) Temperature. (b) z velocity.

Fig. 3 shows the local heat transfer coefficients of both cold and hot sides of supercritical CO_2. Higher heat transfer coefficients are observed at the two channel inlets due to the entrance effect. After that, the heat transfer coefficients keep stable just with a very slow decrease along the flow direction. The increased mass flux leads to steady increase of heat transfer coefficient.

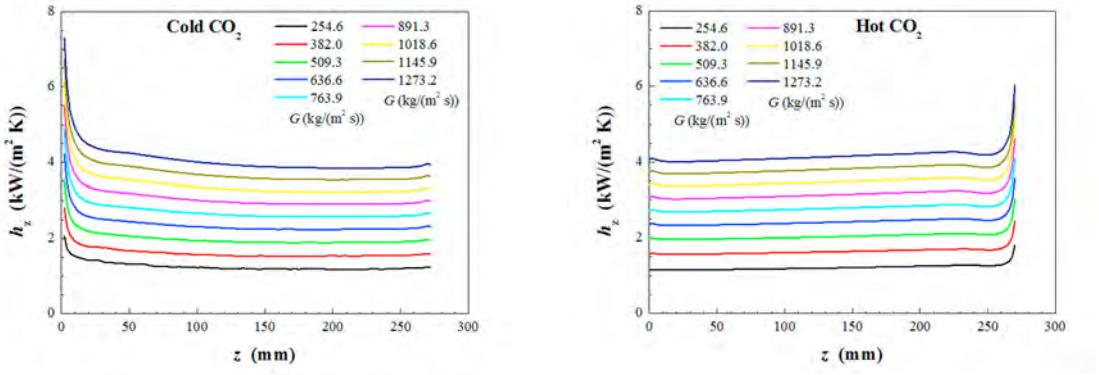

(a) (b)

Fig. 3. Local heat transfer coefficient: (a) Cold side. (b) Hot side.

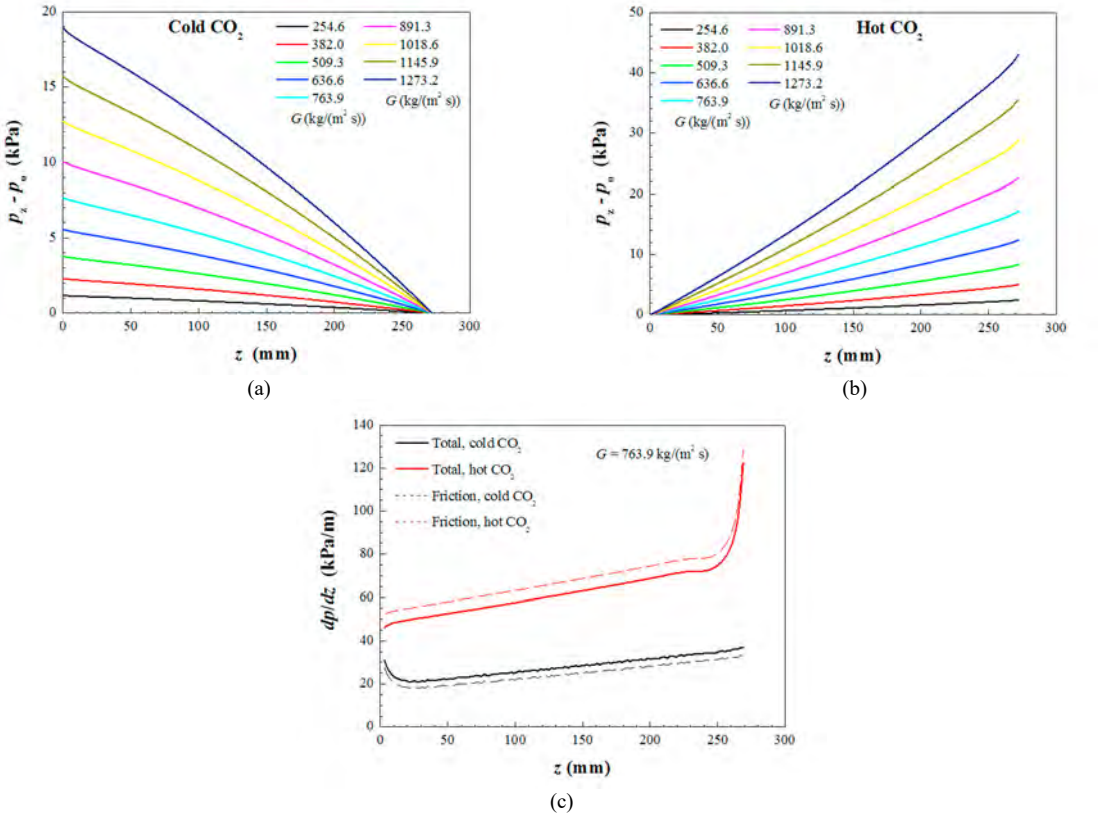

(a) (b)

(c)

Fig. 4. Local pressure drop: (a) Cold side. (b) Hot side. (c) Pressure gradient (G = 763.9 kg/(m^2·s)).

Fig. 4 shows the local pressure drop of both cold and hot sides of supercritical CO_2. On both cold and hot sides, the pressure decreases steadily along the flow direction. A high mass flux results in higher local pressure drop. The pressure gradients show different patterns for cold and hot sides of supercritical CO_2. On the cold side, the pressure gradient drops quickly and then goes up steadily, while on the hot side, the pressure gradient firstly decrease dramatically and continue to decline. The first decrease on the two sides is caused by the entrance effect of the turbulent flow, and the other from the variation of thermophysical properties caused by the changes in temperature.

4.2. Average thermohydraulic performance

Fig. 5 shows the average heat transfer coefficient and pressure drop of both cold and hot sides of supercritical CO_2. For the same mass flux, the average heat transfer coefficient on the two sides are similar to each other, however, the pressure drop is obviously higher for the hot side than the cold side. Higher mass flux results in the increase of heat transfer and pressure drop. For mass flux from 254.6 to 1273.2 kg/(m^2·s), the average heat transfer coefficient increases from 1.26 to 4.09 kW/(m^2·K) on the cold side and 1.22 to 4.18 kW/(m^2·K) on the hot side, while the total pressure drop increases from 1.2 to 18.9 kPa on the cold side and 2.5 to 43.0 kPa on the hot side.

Fig. 6 demonstrates the average Nusselt number and friction factor for both cold and hot sides of supercritical CO_2. For the same average Reynolds number, the average Nusselt number shows almost similar values on the two different sides, and the average friction factor is higher or the cold side of supercritical CO_2 than the hot side. For the mass flux from 254.6 to 1273.2 kg/(m^2·s), the average Reynold number increases from 11757 to 59263 on the cold side and from 11526 to 55769 on the hot side, the average Nusselt number increases from 39.3 to 128.6 on the cold side and 36.9 to 121.0 on the hot side, and the average friction factor decreases from 0.032 to 0.021 on the cold side and 0.026 to 0.018 on the hot side.

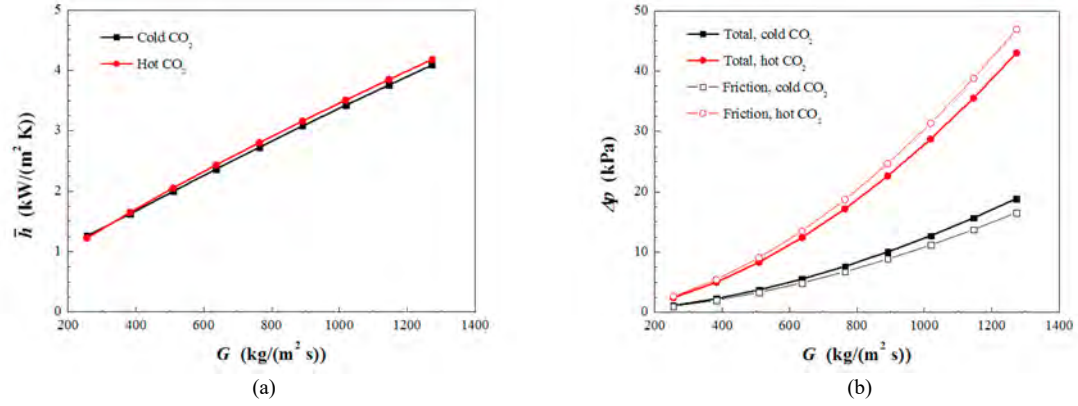

(a) (b)

Fig. 5. Average heat transfer and pressure drop: (a) Heat transfer coefficient. (b) Pressure drop.

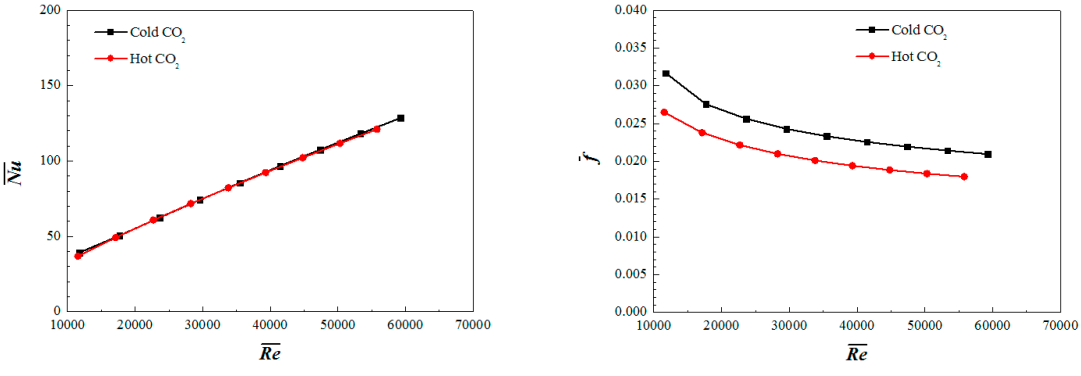

(a) (b)

Fig. 6. Average thermohydraulic performance: (a) Nusselt number. (b) Friction factor.

Fig. 7 indicates the variation of overall heat transfer rate and overall heat transfer coefficient with the mass flux. Increase of mass flux result in steady increase of both overall heat transfer rate and overall heat transfer coefficient.

For the mass flux from 254.6 to 1273.2 kg/(m^2·s), the overall heat transfer rate increases from 96.2 to 393.5 W, and the overall heat transfer coefficient rises from 0.652 to 1.965 kW/(m^2·K).

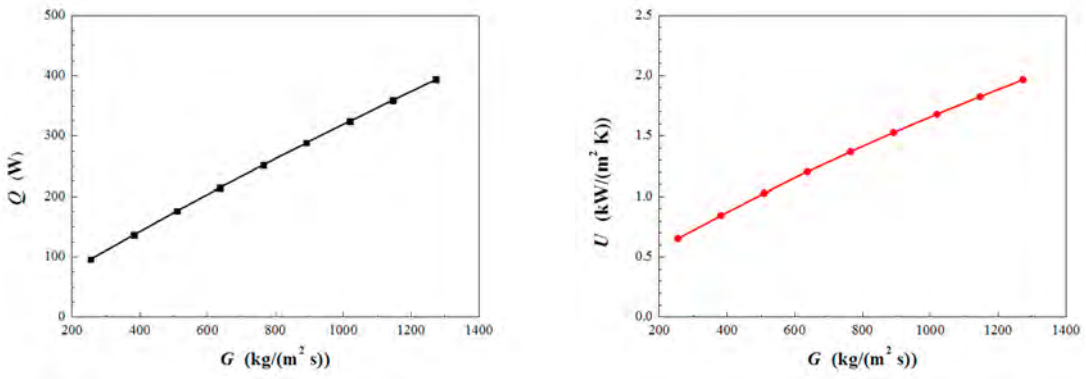

(a) (b)

Fig. 7. Overall thermohydraulic performance: (a) Heat transfer rate. (b) Heat transfer coefficient.

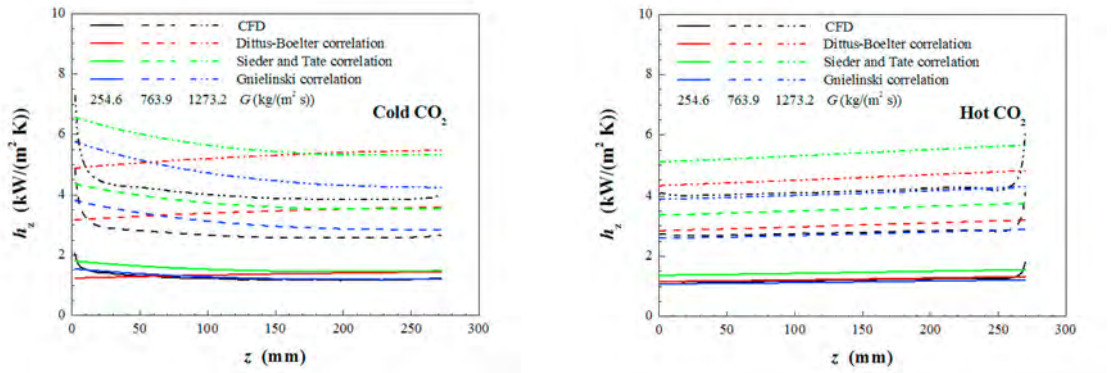

(a) (b)

Fig. 8. Comparison of heat transfer with prediction from empirical correlation: (a) Cold side. (b) Hot side.

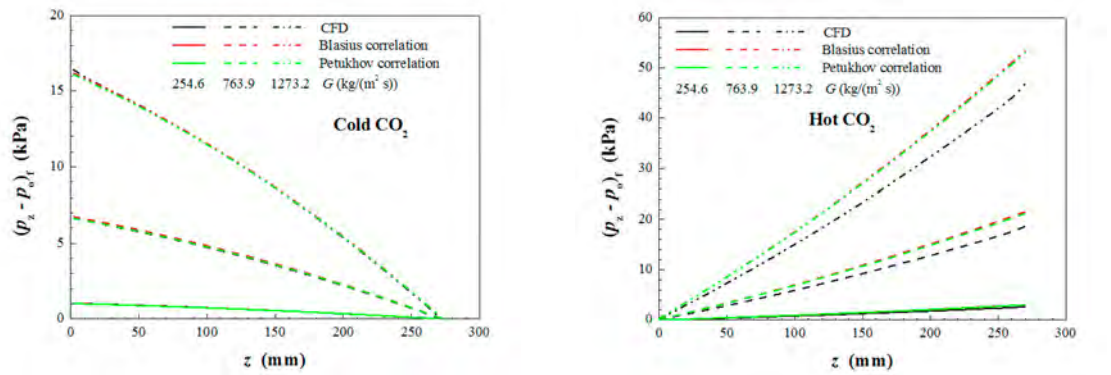

(a) (b)

Fig. 9. Comparison of pressure drop with prediction from empirical correlation: (a) Cold side. (b) Hot side.

4.3. Comparison with prediction from empirical correlations

Three empirical correlations of Nusselt number for turbulent flow in circular tubes from the book Fundamentals of Heat and Mass Transfer [6] are selected to compare the computational fluid dynamics (CFD) heat transfer results, including Dittus-Boelter correlation [7], Sieder and Tate correlation [8] and Gnielinski correlation [9]. As shown in Fig. 8, the Gnielinski correlation presents the best prediction. For the cold side supercritical CO_2, the difference between the CFD results and the predictions from Gnielinski correlation is less than 20 % for the local heat transfer in the stable region, and the difference becomes smaller along the flow direction. For the hot side supercritical CO_2, the Gnielinski correlation can predict the CFD results perfectly, with the difference less than 2 %.

Two empirical correlations of friction factor for turbulent flow in circular tubes are selected to compare the CFD pressure drops, including Blasius correlation and Petukhov correlation [10]. Fig. 9 shows the local friction pressure drop of the CFD results with the predictions from these empirical correlations. The friction pressure drop is obtained by removing the acceleration term from the total pressure drop on the cold side and removing the deceleration term on the hot side. It can be seen that both Blasius correlation and Petukhov correlation can predict the CFD results perfectly for the cold side supercritical CO_2 with difference less than 2.5 %. For the hot side, the Blasius correlation and Petukhov correlation can predict the CFD results with difference less than 15 %.

5. Conclusions

A three-dimensional numerical model is built to investigate the thermohydraulic performance of supercritical CO_2 flow in a printed circuit heat exchanger. This numerical model takes entrance effect, conjugate heat transfer, NIST real gas thermophysical properties and buoyancy effect into account. Based on the numerical results, the following conclusions can be drawn.

Local heat transfer drops quickly near the inlet due to the entrance effect and then keeps steady along the flow direction. Pressure gradients rise with the increased temperature of supercritical CO_2. Larger mass flux results in increase of heat transfer and pressure drop. For the mass flux from 254.6 to 1273.2 kg/(m^2·s), the overall heat transfer rate increases from 96.2 to 393.5 W, and the overall heat transfer coefficient rises from 0.652 to 1.965 kW/(m^2·K). Gnielinski correlation can predict the heat transfer well and the difference with the CFD result is less than 20 % for the cold side of supercritical CO_2 and 2 % for the hot side. Both Blasius correlation and Petukhov correlation can predict pressure drop well with a difference less than 2.5 % for the cold side of supercritical CO_2 and 15 % for the hot side.

Acknowledgements

The work presented in this paper is supported by a number of funders as follows: (i) Research Councils UK Centre for Sustainable Energy Use in Food Chains, grant no. EP/K011820/1, EPSRC project ‘Optimising Energy Management in Industry - OPTEMIN', grant No. EP/P004636/1, and the European Union’s Horizon 2020 research and innovation programme under grant agreement No. 680599. The Authors would like to acknowledge the financial support received by the project funders and the industry partners. The data used in the analysis are given in the paper but if more data or information is required they can be obtained by contacting the corresponding author.

References

[1] Fundamentals and applications of supercritical carbon dioxide (sCO_2) based power cycles. Woodhead Publishing, 2017.
[2] Compact heat exchangers a training package for engineers. Energy Efficiency Office, London, UK, 2000.
[3] Kruizenga A, Anderson M, Fatima R, et al. Heat transfer of supercritical carbon dioxide in printed circuit heat exchanger geometries. *Journal of Thermal Science and Engineering Applications*, 2011, 3(3): 031002.
[4] Kruizenga A, Li H, Anderson M, et al. Supercritical carbon dioxide heat transfer in horizontal semicircular channels. *Journal of Heat transfer*, 2012, 134(8): 081802.
[5] Li H, Kruizenga A, Anderson M, et al. Development of a new forced convection heat transfer correlation for CO_2 in both heating and cooling modes at supercritical pressures. *International Journal of Thermal Sciences*, 2011, 50(12): 2430-2442.
[6] Bergman T L, Lavine A S, Incropera F P, DeWitt D P, Fundamentals of heat and mass transfer. John Wiley & Sons, 2011.

[7] Winterton R H S. Where did the Dittus and Boelter equation come from?. *International Journal of Heat and Mass Transfer*, 1998, 41(4-5): 809-810.
[8] Sieder E N, Tate G E. Heat transfer and pressure drop of liquids in tubes. *Industrial & Engineering Chemistry*, 1936, 28(12): 1429-1435.
[9] Gnielinski V. New equations for heat and mass transfer in turbulent pipe and channel flow. *International Chemical Engineering*, 1976, 16(2): 359-368.
[10] Petukhov B S, Kirillov P L. About heat transfer at turbulent fluid flow in tubes. *Thermal Engineering*, 1958, 4: 63-68.